Fusion barriers using the energy-density formalism: Simple analytical formula and the calculation of fusion cross sections

Rajeev K. Puri* and Raj K. Gupta†
Physics Department, Panjab University, Chandigarh 160014, India
(Received 9 October 1991)

Fusion barriers are calculated within the sudden approximation, using the Skyrme interaction energy-density model. Both the closed and unclosed shell nuclei are considered and the role of spin-density term is studied in detail. For unclosed shell nuclei, the fusion cross sections are found to decrease by as much as ~ 50 mb when spin-density effects are included. Very accurate, simple analytical expressions, in terms of only the masses and charges of the reacting nuclei, are obtained for the barrier heights and positions. This introduces a great simplification for the fusion barrier calculations.

PACS number(s): 25.70.−z, 25.70.Jj

I. INTRODUCTION

It is now well accepted [1–3] that the fusion threshold energy or the height of fusion barrier (also called, interaction barrier) cannot be given only by the Coulomb barrier. The nuclear interactions play an equally important role in determining such a barrier. Thus, in order to be able to calculate the total interaction potential, $V(R)=V_C(R)+V_N(R)$, analytically, one of the problems of interest is to obtain an analytical expression for the equivalent nuclear proximity potential. Some work was already done [4–7] in this direction, using the energy-density formalism (EDF). Alternatively, it is of interest to obtain analytical expressions for the interaction barrier heights and positions, whose predictions can be compared with the empirical estimates [8] from measured cross sections. Such information is required for calculating the excitation functions, etc.

Fusion barriers have been defined in many ways. We use here the very much used definition [4–8], as the height of interaction potential $V(R)$, where the slope

$$\left[\frac{dV(R)}{dR}\right]_{R=R_B}=0, \quad \left[\frac{d^2V(R)}{dR^2}\right]_{R=R_B}<0 . \tag{1}$$

This means that the fusion barrier is defined with its position at the distance $R=R_B$, and the height $V(R=R_B)=V_B$. Figure 1 illustrates our calculated interaction potential $V(R)$ for the $^{16}O+^{16}O$ reaction, using the EDF with Skyrme force parameters of force SIII and $\lambda=0$ (see below for notations). The nuclear and Coulomb potentials are also shown separately. At $R=R_B$, the difference ΔV gives the contribution of nuclear potential to the fusion barrier V_B. In this figure, we have also shown the so-called "effective radius," R_{eff}. This is defined as the value of R at which the fusion barrier $V_B=V_C$, the Coulomb potential. By using this definition, apparently one almost neglects the contribution of nuclear potential and obtains fusion radii larger than R_B. Defining further,

$$V_B=\frac{Z_1Z_2e^2}{R_{\text{eff}}}, \quad R_{\text{eff}}=r_{\text{eff}}(A_1^{1/3}+A_2^{1/3}) , \tag{2}$$

many experiments have been analyzed [9,10], by taking Eq. (2) as the effective interaction barrier. However, r_{eff} does not take a constant value (see Fig. 7 below), against the expectations of these authors.

Using the energy-density formalism, fusion barriers have been calculated [11,12] for a large number of target-projectile combinations. Calculations are made within the sudden approximation, using the energy-density functionals due to Brueckner *et al.* [13] and the Skyrme density-dependent interaction [14]. For the latter case, fusion barriers are calculated [12] only for combinations of the closed shell nuclei. This is because the spin density $\mathbf{J}=0$ for closed shell nuclei (called spin-saturated nuclei) and, until recently, the required expression of $\mathbf{J}$ for unclosed shell nuclei were not available. In a recent paper [15], we have derived a general expression of $\mathbf{J}$ for nuclei with any number of valence particles (or holes) outside the closed core. A first calculation of fusion barriers and cross sections for the spin-unsaturated nuclei was also published very recently [16].

The aim of this paper is at least threefold: First, we extend our calculations of Ref. [16] to a larger number of nuclei, up to about $f_{7/2}$- shell, and to combinations of very spin-unsaturated nuclei. This allows us to study the contribution of spin density in fusion barrier heights and positions. Secondly, almost for the first time, we obtain a

*Present address: Institut für Theoretische Physik, Universität Tübingen, D-7400 Tübingen 1, Germany.
†Presently visiting: Institut für Theoretische Physik, Johann Wolfgang Goethe-Universität, D-6000 Frankfurt am Main, Germany.

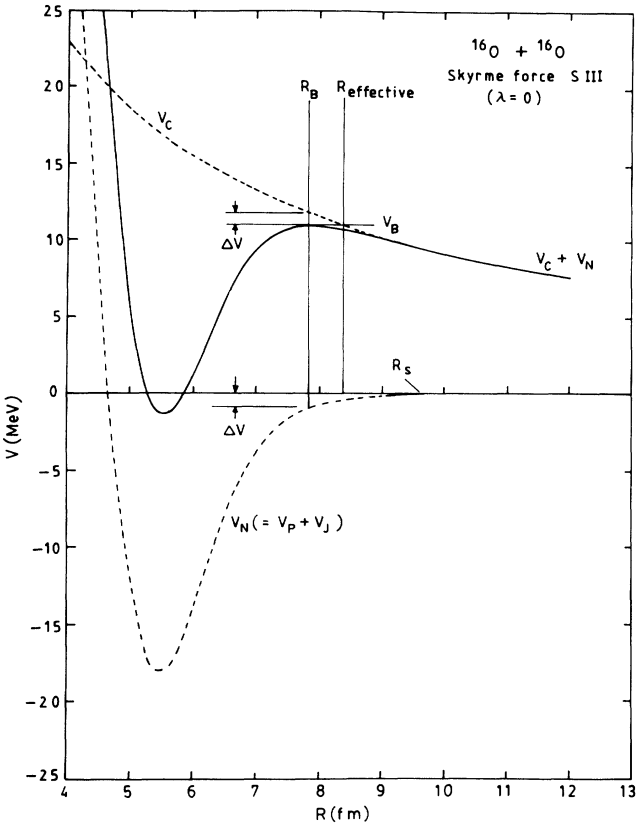

FIG. 1. Interaction potential $V(R)=V_C(R)+V_N(R)$ for the reaction $^{16}O+^{16}O$, using the energy-density model with Skyrme force SIII and the surface correction coefficient $\lambda=0$. Separate Coulomb and nuclear contributions are also shown. ΔV is the contribution of nuclear potential V_N to the barrier V_B at $R=R_B$. The radius R_{eff} is the value of R at $V_B=V_C$.

simple analytical expression for calculating the interaction barriers from the knowledge of only the masses and charges of colliding nuclei [17]. Finally, we calculate the fusion cross sections and analyze the role of spin-density term on the fusion cross sections (see also Ref. [16]).

In Sec. II we give a brief description of the formalism used and approximations made for the densities and forces, etc. Section III gives our calculations for (i) fusion barriers, compared with empirical estimates and other available calculations, (ii) the analytical formulas for barrier heights and positions, and (iii) the calculations of fusion cross sections, compared with experimental data. In all cases the role of spin-density term is also studied. A summary of our results is given in Sec. IV.

II. THE FORMALISM

The fusion cross section σ_f is considered to account entirely for the process of compound nucleus formation and is made up of two components: the fusion evaporation σ_{evap} and fusion fission σ_{fiss}. At low incident energies and for light heavy-ion collisions, σ_{evap} is taken to represent the fusion cross section σ_f, which for energies above the barrier ($E_{\text{c.m.}} > V_B$) is well described by the sharp cutoff model expression

$$\sigma_f = \pi R_B^2 (1 - V_B / E_{\text{c.m.}}) . \tag{3}$$

We use this expression in the following, with barrier heights V_B and positions R_B calculated in Skyrme interaction energy-density formalism [18]. The energy dependence can also be introduced in the barrier by adding to the potential $V(R)$ the centrifugal potential V_l due to angular momentum l. The effect of this term on Eq. (3) is known [19] to reduce the fusion cross sections and in the following we take $l=0$ for simplicity.

Using the Skyrme interaction, Vautherin and Brink [14] have derived the energy-density functional $H(\mathbf{r})$ for a system whose ground state is represented by a Slater determinant and the subspace of occupied single-particle states is invariant under time reversal. For an even-even spherical nucleus, this has the form (the subscripts n and p refer to neutrons and protons, respectively)

$$\begin{aligned} H(\rho,\tau,\mathbf{J}) = {} & \frac{\hbar^2}{2m}\tau + \tfrac{1}{2}t_0[(1+\tfrac{1}{2}x_0)\rho^2 - (x_0+\tfrac{1}{2})(\rho_n^2+\rho_p^2)] + \tfrac{1}{4}(t_1+t_2)\rho\tau \\ & + \tfrac{1}{8}(t_2-t_1)(\rho_n\tau_n+\rho_p\tau_p) + \tfrac{1}{16}(t_2-3t_1)\rho\nabla^2\rho + \tfrac{1}{32}(3t_1+t_2)(\rho_n\nabla^2\rho_n+\rho_p\nabla^2\rho_p) \\ & + \tfrac{1}{4}t_3\rho_n\rho_p\rho + \tfrac{1}{16}(t_1-t_2)(\mathbf{J}_n^2+\mathbf{J}_p^2) - \tfrac{1}{2}W_0(\rho\nabla\cdot\mathbf{J}+\rho_n\nabla\cdot\mathbf{J}_n+\rho_p\nabla\cdot\mathbf{J}_p) . \end{aligned} \tag{4}$$

Here, t_0, x_0, t_1, t_2, t_3, and W_0 are the Skyrme interaction parameters, obtained by different authors [14,20–26] to fit the various ground-state properties of the nuclei and $\rho=\rho_n+\rho_p$, $\tau=\tau_n+\tau_p$, and $\mathbf{J}=\mathbf{J}_n+\mathbf{J}_p$.

Knowing $H(\mathbf{r})$, the energy-density model defines the nucleus-nucleus interaction potential as the difference between the energy expectation value $E=\int H(\mathbf{r})d\mathbf{r}$ of the colliding nuclei at a finite separation R and at infinity,

$$V_N(R) = E(R) - E(\infty) = \int \{H(\rho,\tau,\mathbf{J}) - [H_1(\rho_1,\tau_1,\mathbf{J}_1) + H_2(\rho_2,\tau_2,\mathbf{J}_2)]\} d\mathbf{r} . \tag{5}$$

This means that the two nuclei form a composite system at R and are completely separated at infinity. Also, $\rho=\rho_1+\rho_2$, $\tau=\tau_1+\tau_2$, $\mathbf{J}=\mathbf{J}_1+\mathbf{J}_2$ refer to the sudden approximation, which means neglecting exchange effects due to antisymmetrization. Brink and Stancu [6,12] have shown that such antisymmetrization effects can be assimilated reasonably well by using for τ, the Thomas-Fermi (TF) kinetic energy density τ_{TF} corrected for addi-

TABLE I. Calculated fusion barrier heights and positions in energy-density model using Skyrme force SIII ($\lambda=0$), compared with the empirical data and the models other than the energy-density model. The systems are listed with respect to their increasing Z_1Z_2 values.

System	Z_1Z_2	Present				Empirical		Ref.	Other models		Ref.
		V_C	V_N	V_B	R_B	V_B	R_B		V_B	R_B	
$^{12}C+^{12}C$	36	6.91	−0.46	6.45	7.50	5.80±0.3	6.50±0.4	[30]	6.32	7.42	[8]
						6.37	7.34	[8]	5.61	8.77	[8]
$^{12}C+^{16}O$	48	8.98	−0.57	8.41	7.70	7.70±0.4	7.50±0.3	[30]	8.00	7.90	[43]
						7.94±0.15	7.23±0.24	[41]			
$^{12}C+^{18}O$	48	8.66	−0.61	8.05	7.98	7.70±0.2	7.90±0.3	[30]	7.80	8.10	[43]
						7.55±0.11	7.45±0.20	[41]			
$^{16}O+^{16}O$	64	11.67	−0.70	10.97	7.90	11.20±0.6	7.60±0.4	[30]	10.86	7.67	[47]
						10.91	8.20	[43]	10.40	8.10	[43]
						11.00	7.60	[32]	11.10	8.31	[46]
$^{12}C+^{24}Mg$	72	12.45	−0.92	11.53	8.33	11.60±0.5	7.50±0.3	[44]			
						12.23±0.3	7.97±0.2	[45]			
$^{12}C+^{26}Mg$	72	12.28	−0.94	11.34	8.44	11.50±0.5	8.40±0.3	[44]			
$^{16}O+^{20}Ne$	80	13.77	−0.96	12.81	8.37	13.40	8.22	[48]			
$^{12}C+^{28}Si$	84	14.31	−1.11	13.20	8.45	12.59±0.3	7.42±0.2	[45]	16.00	7.57	[46]
$^{12}C+^{30}Si$	84	14.22	−1.14	13.08	8.51	13.20	8.39	[8]	13.13	9.08	[46]
$^{16}O+^{24}Mg$	96	16.40	−1.33	15.07	8.43	15.90±0.9	8.40±0.4	[44]	15.00	8.60	[43]
						16.00	8.48	[43]	15.87	7.97	[47]
$^{16}O+^{26}Mg$	96	16.00	−1.17	14.83	8.64	16.50±0.9	8.70±0.4	[44]	17.09	8.10	[46]
$^{18}O+^{24}Mg$	96	15.86	−1.31	14.55	8.71	14.90±0.9	7.80±0.3	[30]	14.70	8.70	[43]
						14.80	7.82	[43]			
$^{20}Ne+^{20}Ne$	100	16.49	−1.31	15.18	8.73	15.20	8.42	[48]			
$^{12}C+^{40}Ar$	108	17.59	−1.22	16.38	8.84	16.20±0.2		[56]			
$^{16}O+^{28}Si$	112	18.86	−1.61	17.25	8.55	17.23	7.98	[43]	17.20	8.60	[43]
									18.18	8.46	[47]
$^{18}O+^{28}Si$	112	18.06	−1.38	16.68	8.93	16.90	8.76	[8]	16.20	9.44	[8]
$^{16}O+^{40}Ar$	144	23.19	−1.77	21.42	8.94	21.00±0.3		[56]			
$^{24}Mg+^{24}Mg$	144	23.14	−1.96	21.19	8.96	21.53±0.5	8.37±0.2	[45]			
						22.30±0.4	8.90±0.3	[44]			
$^{24}Mg+^{26}Mg$	144	22.86	−1.98	20.88	9.07	20.80±0.5	8.33±0.2	[45]			
$^{16}O+^{40}Ca$	160	25.77	−1.79	23.98	8.94	23.70±1.0	9.00±0.4	[30]	23.70	8.90	[43]
						23.70	9.03	[43]	24.63	8.59	[47]
$^{24}Mg+^{28}Si$	168	26.94	−2.55	24.39	8.98	24.64±0.6	8.11±0.2	[45]			
$^{24}Mg+^{32}S$	192	30.42	−2.74	27.68	9.09	28.10±1.6	8.70±0.3	[44]	28.18	9.10	[42]
						27.93	9.20	[42]	29.40	8.52	[47]
									28.80	8.90	[11]
$^{24}Mg+^{34}S$	192	29.78	−2.41	27.37	9.29	27.38	9.40	[42]	27.88	9.21	[42]
$^{26}Mg+^{32}S$	192	30.05	−2.76	27.29	9.20	27.48	9.36	[42]	27.80	9.24	[42]
$^{26}Mg+^{34}S$	192	29.43	−2.43	27.00	9.40	27.11	9.50	[42]	27.50	9.35	[42]
$^{28}Si+^{28}Si$	196	31.02	−2.90	28.12	9.10	28.89	8.94	[50]	29.60	9.08	[50]
						28.95±0.7	8.25±0.2	[45]	29.83	8.63	[50]
$^{28}Si+^{30}Si$	196	30.50	−2.68	27.82	9.26	29.13	8.86	[50]	29.27	8.82	[50]
						28.28±0.7	8.47±0.2	[45]	29.38	8.75	[50]
$^{30}Si+^{30}Si$	196	30.32	−2.78	27.54	9.31	28.54	9.06	[50]	28.64	9.02	[50]
$^{20}Ne+^{40}Ca$	200	31.29	−2.64	28.64	9.21	28.60	9.32	[49]	28.23	9.64	[8]
$^{32}S+^{40}Ca$	320	48.51	−4.21	44.30	9.50	43.30±4.5	9.00±0.7	[30]	45.80	9.30	[11]
									42.50	9.26	[51]
$^{28}Si+^{58}Ni$	392	58.01	−5.34	52.67	9.73	53.80±0.8	9.00±0.9	[55]	54.44	9.56	[55]
$^{28}Si+^{62}Ni$	392	57.02	−4.96	52.06	9.90	52.89	9.89	[55]	53.74	9.70	[55]
$^{28}Si+^{64}Ni$	392	56.82	−5.07	51.76	9.93	52.40±1.1	9.20±1.0	[55]	53.42	9.76	[55]
$^{30}Si+^{58}Ni$	392	57.10	−5.00	52.10	9.89	52.20±1.2	8.30±1.1	[55]	53.82	9.68	[55]
$^{30}Si+^{62}Ni$	392	56.14	−4.63	51.51	10.05	52.20±0.9	9.70±1.0	[55]	53.15	9.82	[55]
$^{30}Si+^{64}Ni$	392	55.95	−4.73	51.22	10.09	51.20±0.9	9.40±0.8	[55]	52.84	9.88	[55]
$^{40}Ca+^{40}Ca$	400	59.50	−5.25	54.26	9.68	50.60±2.8	9.50±0.5	[30]	55.03	9.74	[52]
						52.30±0.5	8.80±0.5	[53]	53.20		[54]
						55.60±0.8	9.10±0.6	[37]			
$^{40}Ca+^{44}Ca$	400	58.05	−4.64	53.41	9.92	51.70±1.2	8.50±0.5	[53]	54.35	9.88	[52]
									55.00		[53]

TABLE I. (*Continued*).

System	Z_1Z_2	Present				Empirical		Ref.	Other models		Ref.
		V_C	V_N	V_B	R_B	V_B	R_B		V_B	R_B	
									54.00		[53]
$^{40}Ca+^{48}Ca$	400	57.23	−4.63	52.60	10.06	51.30±1.0	7.80±0.3	[53]	54.08	9.93	[52]
									54.30		[43]
$^{32}S+^{58}Ni$	448	65.56	−5.86	59.70	9.84	59.80±1.4	8.60±0.9	[55]	61.80	9.70	[11]
						59.50	8.50±0.3	[46]	59.20		[34]
$^{32}S+^{64}Ni$	448	64.23	−5.55	58.68	10.04	58.10±0.7	8.80±0.5	[55]	60.36	9.88	[55]
$^{34}S+^{58}Ni$	448	64.93	−5.89	59.04	9.94	58.40±1.4	7.50±0.9	[55]	60.88	9.79	[55]
$^{34}S+^{64}Ni$	448	63.00	−4.94	58.06	10.24	57.20±0.6	8.90±0.6	[55]	59.78	9.99	[55]
$^{36}S+^{58}Ni$	448	63.68	−5.23	58.45	10.13	58.00±1.1	7.50±0.6	[55]	60.30	9.90	[55]
$^{36}S+^{64}Ni$	448	62.43	−4.93	57.50	10.33	56.70±1.0	8.80±0.6	[55]	59.24	10.09	[55]
$^{40}Ar+^{58}Ni$	504	71.01	−5.73	65.28	10.22	65.30±0.5		[56]			
$^{40}Ar+^{60}Ni$	504	70.77	−5.83	64.95	10.25	65.50±0.6		[56]			
$^{40}Ar+^{62}Ni$	504	70.54	−5.96	64.57	10.29	65.10±0.6		[56]			
$^{40}Ar+^{64}Ni$	504	69.62	−5.40	64.22	10.42	63.90±0.5		[56]			
$^{40}Ca+^{58}Ni$	560	80.48	−7.32	73.16	10.02	73.36	10.20	[8]	73.57	10.31	[8]
$^{40}Ca+^{62}Ni$	560	79.14	−6.80	72.34	10.19	72.30	10.35	[8]	72.87	10.42	[8]
$^{58}Ni+^{58}Ni$	784	110.04	−11.01	99.03	10.26	97.90	8.30	[57]	95.90		[54]
$^{58}Ni+^{64}Ni$	784	106.87	−9.57	97.30	10.56	96.00	8.20	[57]	94.10		[54]
$^{64}Ni+^{64}Ni$	784	104.84	−9.15	95.69	10.77	93.50	8.60	[57]			

tional surface effects. We take

$$\tau=\tau_{\rm TF}+\lambda\frac{(\nabla\rho)^2}{\rho}\ , \tag{6}$$

where $\tau_{\rm TF}=\frac{3}{5}(\frac{3}{2}\pi^2)^{2/3}\rho^{5/3}$ and the surface correction is due to von Weizsäcker [27], with λ having values between $\frac{1}{4}$ and $\frac{1}{36}$. Equation (6) makes the energy density (4) a functional of ρ and **J** only, which allows us to calculate (5) simply as

$$V_N(R)=V_P(R)+V_J(R)\ . \tag{7}$$

Here, $V_P(R)$ is the $\mathbf{J}=0$, ρ-dependent part of the interaction potential and $V_J(R)$, the spin-density-dependent part. Notice that $V_J(R)$ also depends on ρ. We have solved [15] for $V_P(R)$ directly in the proximity force theorem as

$$V_P(R)=\int\{H(\rho)-[H_1(\rho_1)+H_2(\rho_2)]\}d\mathbf{r}$$
$$=2\pi\frac{C_1C_2}{C_1+C_2}\Phi(s)\ , \tag{8}$$

where C_i are the Süssman central radii and the universal function [28]

$$\Phi(s)=\int_{s_0}^{\infty}e(s)ds$$
$$=\int\{H(\rho)-[H_1(\rho_1)+H_2(\rho_2)]\}dZ\ . \tag{9}$$

TABLE II. Comparisons of some theoretical barrier heights and positions calculated in energy-density model, using Skyrme force SIII.

System	Present		Empirical		Stancu-Brink [12]		Brink-Stancu [6]		Behera *et al.* [58]	
	R_B	V_B	R_B	V_B	R_B	V_B	R_B	V_B	R_B	V_B
$^{16}O+^{16}O$	7.90	10.97	7.60±0.4	11.20±0.6	7.70	11.06	8.10	10.41	7.70	11.11
			7.60	11.00						
$^{16}O+^{40}Ca$	8.94	23.98	9.00±0.4	23.70±1.0	8.50	25.12	8.80	24.04	8.50	25.19
			9.03	23.70						
$^{16}O+^{48}Ca$	9.22	23.20			8.80	24.32	9.10	23.33	8.80	24.50
$^{16}O+^{56}Ni$	9.21	32.28			8.80	33.91	9.10	32.74	8.70	34.20
$^{40}Ca+^{40}Ca$	9.68	54.26	8.80±0.5	52.3±0.5	9.25	57.76	9.50	55.92	9.20	58.01
			9.10±0.6	55.60±0.8						
$^{40}Ca+^{48}Ca$	10.06	52.60	7.80±0.3	51.30±1.0	9.60	56.05	9.80	54.31	9.50	56.52
$^{40}Ca+^{56}Ni$	9.95	73.72			9.50	78.36	9.80	76.27	9.40	79.14
$^{48}Ca+^{48}Ca$	10.45	51.05			9.90	54.58	10.10	53.22		
$^{48}Ca+^{56}Ni$	10.33	71.50			9.90	76.08	10.10	74.11		

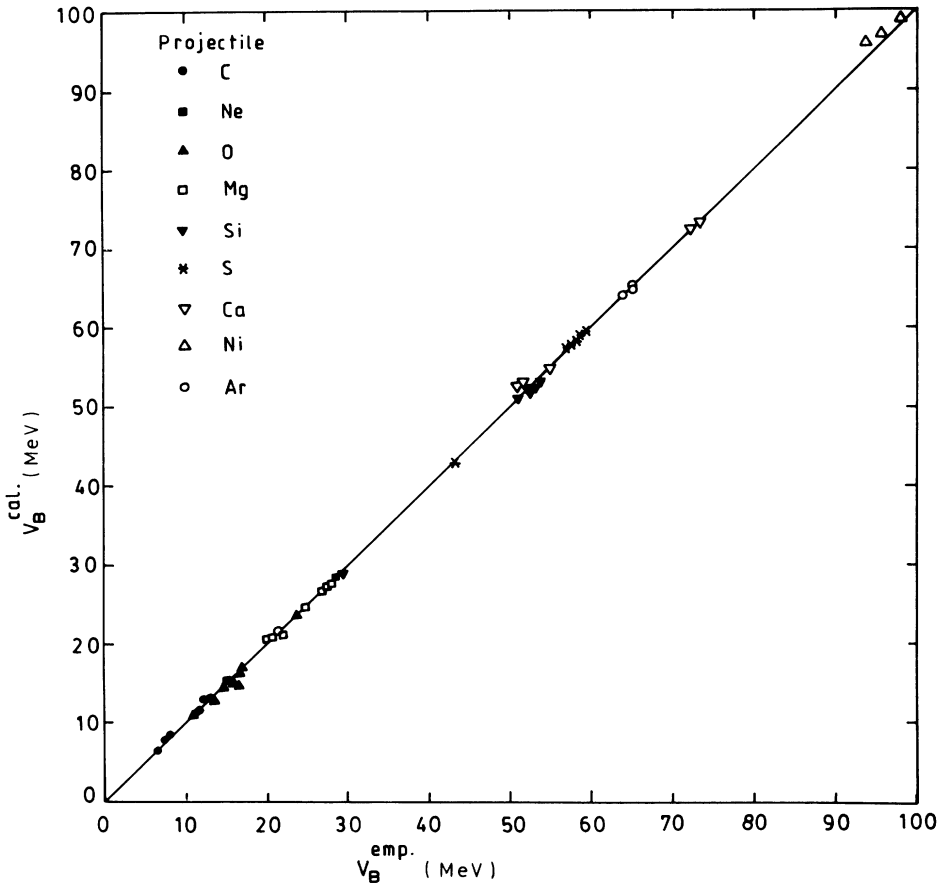

FIG. 2. Comparisons between the empirical and our calculated barrier heights V_B, using Skyrme force SIII ($\lambda=0$). The calculated data are also given in Table I and the symbols are explained in the body of figure. The solid line is a straight-line fit to the data.

Here, $s=R-C_1-C_2$, with its minimum value s_0, and $e(s)$ is the interaction energy per unit area between two flat slabs of semi-infinite nuclear matter with surfaces parallel to the X-Y plane, moving in the Z direction. For the nucleon density ρ, we have used the two-parameter Fermi density distribution ($i=1,2$):

$$\rho_i(Z_i)=\rho_{0i}\left[1+\exp\left[\frac{Z_i-C_i}{a_i}\right]\right]^{-1}, \quad -\infty \le Z \le \infty \tag{10}$$

TABLE III. Comparisons of our calculated barrier heights with other model calculations taken from the compilation of Vaz *et al.* [8].

System	Present	Empirical	Barrier heights V_B Krappe	Proximity	Ngô *et al.*	Ngô-Ngô	Folding
$^{12}C+^{12}C$	6.45	6.37	5.96	6.32	5.61	5.91	6.27
$^{12}C+^{16}O$	8.41	8.09	7.80	8.25	7.37	7.75	8.07
$^{12}C+^{28}Si$	13.20	14.53	13.08	13.75	12.47	13.04	13.47
$^{12}C+^{30}Si$	13.08	13.20	12.92	13.56	12.36	12.89	13.33
$^{16}O+^{16}O$	10.97	10.85	10.21	10.78	9.69	10.18	10.40
$^{16}O+^{24}Mg$	15.07	15.26	14.88	15.62	14.20	14.86	15.05
$^{16}O+^{28}Si$	17.25	17.00	17.15	17.96	16.40	17.14	17.40
$^{16}O+^{40}Ca$	23.98	23.06	23.72	24.72	22.84	23.75	23.83
$^{18}O+^{28}Si$	16.68	16.90	16.86	17.61	16.20	16.84	16.81
$^{20}Ne+^{40}Ca$	28.64	28.41	29.24	30.37	28.23	29.33	29.04
$^{28}Si+^{28}Si$	28.12	28.67	28.84	29.98	27.82	28.94	29.19
$^{32}S+^{24}Mg$	27.68	28.28	28.28	29.40	27.26	28.36	28.28
$^{32}S+^{40}Ca$	44.30	43.92	45.20	46.63	43.96	45.48	45.00
$^{32}S+^{58}Ni$	59.70	61.91	60.87	62.41	59.68	61.37	60.94
$^{40}Ar+^{58}Ni$	65.28	66.32	66.74	68.18	65.78	67.32	66.51
$^{40}Ca+^{58}Ni$	73.16	73.36	74.75	76.37	73.57	75.47	74.72
$^{40}Ca+^{62}Ni$	72.34	72.30	73.89	75.39	72.87	74.54	73.64

with $Z_2=R-Z_1$ for motion in the Z direction in a plane. This density gives results that are identical with the microscopic shell-model density and is more realistic for heavy-ion collisions because it does not drop sharply to zero like the TF density distribution. We obtain [15]

$$\Phi(s)=\frac{3}{5}\frac{\hbar^2}{2m}(\tfrac{3}{2}\pi^2)^{2/3}I_{[5/3]}+\tfrac{3}{8}t_0I_{[2]}+\tfrac{1}{16}t_3I_{[3]}+\tfrac{1}{16}(3t_1+5t_2)\tfrac{3}{5}(\tfrac{3}{2}\pi^2)^{2/3}I_{[8/3]}+\Phi_{s\rho}+\Phi_{s\tau_\lambda} \tag{11}$$

with

$$I_{[n]}=\int\{\rho^n-[\rho_1^n+\rho_2^n]\}dZ_1 ,$$

$$\Phi_0=\int\{\rho'^2-[\rho_1'^2+\rho_2'^2]\}dZ_1 ,$$

$$\rho'=\left|\frac{\partial\rho}{\partial Z_1}\right| , \text{ etc. ;}$$

$$\Phi_{s\rho}=\tfrac{1}{64}(9t_1-5t_2)\Phi_0 ,$$

$$\Phi_{s\tau_\lambda}=\tfrac{1}{16}(3t_1+5t_2)\lambda\Phi_0+\frac{\hbar^2}{2m}\lambda\left\{\int\left[\frac{\rho'^2}{\rho}-\left[\frac{\rho_1'^2}{\rho_1}+\frac{\rho_2'^2}{\rho_2}\right]\right]dZ_1\right\} .$$

This equation is solved numerically for the Fermi density (10), using $\rho_n=\rho_p$. For the spin-density-dependent part of the interaction potential, using $\rho_n=\rho_p=(\frac{1}{2}\rho)$, we get from (4) and (5)

$$V_J(R)=\int\{H(\mathbf{J})-[H_1(\mathbf{J}_1)+H_2(\mathbf{J}_2)]\}d\mathbf{r}=-\tfrac{3}{4}W_0\int(\rho_2\nabla\cdot\mathbf{J}_1+\rho_1\nabla\cdot\mathbf{J}_2)d\mathbf{r} . \tag{12}$$

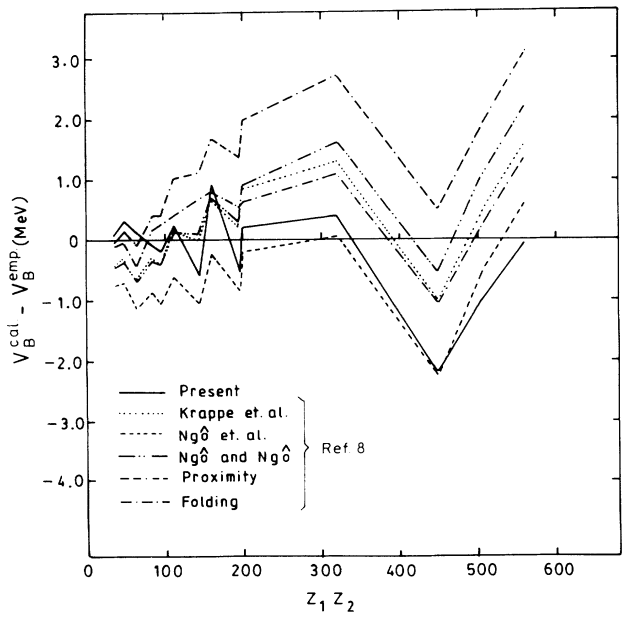

FIG. 3. The deviations between the calculated and empirical barrier heights V_B as a function of Z_1Z_2, for various model calculations. The data are from the compilation of Vaz *et al.* [8] and are also given in Table III.

Notice that here we have not included the term $\frac{1}{16}(t_1-t_2)(\mathbf{J}_n^2+\mathbf{J}_p^2)$, since its contribution is found to be small [29]. In terms of the single-particle orbitals ϕ_i, that define a Slater determinant, the spin density $\mathbf{J}$ is defined as

$$\mathbf{J}_q(\mathbf{r})=(-i)\sum_{i,s,s'}\phi_i^*(\mathbf{r},s,q)[\nabla\phi_i(\mathbf{r},s',q)\times\langle s|\sigma|s'\rangle] . \tag{13}$$

Here, s and q ($=n$ or p) represent the spin and isospin indices, respectively, and the summation i runs over all the occupied single-particle orbitals. For ϕ_i, we use the ansatz [14,15]

$$\phi_i(\mathbf{r},s,q)=\frac{R_\alpha(r)}{r}\sum_{m_lm_s}\langle l\tfrac{1}{2}m_lm_s|jm\rangle Y_l^{m_l}(\hat{\mathbf{r}})\chi_{m_s}(s)\chi_q(t), \tag{14}$$

where $\alpha\equiv q,n,l$ and $R_\alpha(r)=C_{nl}r^{l+1}e^{-\nu r^2}v_{nl}(2\nu r^2)$ is the shell-model, normalized radial wave function, with $\nu=m\omega/2\hbar$ (fm^{-2}). The constant C_{0l} varies smoothly with mass number A of the nucleus, only within a shell [7].

For an even-even nucleus with n_v valence particles (or holes) outside the closed shells, we divide [15] $\mathbf{J}_q(\mathbf{r})$ into two parts (for $q=n$ or p): one due to the core consisting of closed shells and another due to the valence n_v particles (+sign) or holes (−sign),

$$\mathbf{J}(\mathbf{r})=\mathbf{J}_C(\mathbf{r})\pm\mathbf{J}_{n_v}(\mathbf{r}) . \tag{15}$$

Considering that valence nucleons couple to zero angular

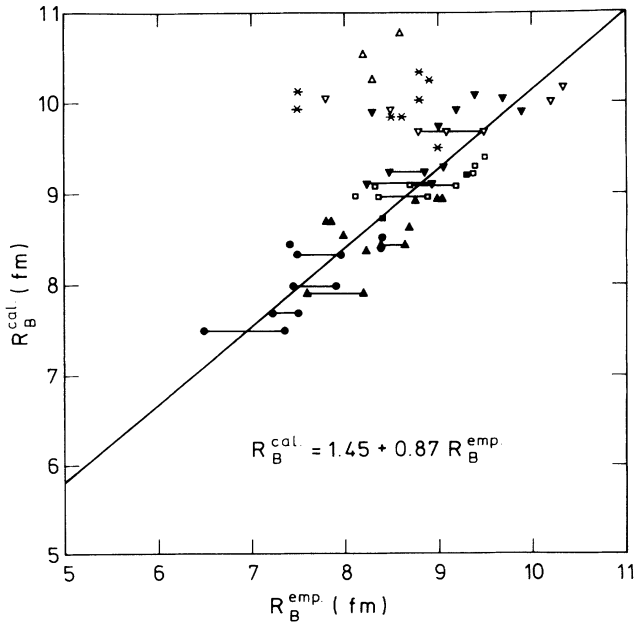

FIG. 4. Same as Fig. 2, but for barrier positions R_B. The multiple empirical estimates are joined by straight lines.

TABLE IV. Effect of spin-density term on fusion barriers, for the Skyrme force SIII ($\lambda=0$). The systems are listed with respect to their increasing Z_1Z_2 values.

System	Z_1Z_2	Without spin-density V_B (MeV)	Without spin-density R_B (fm)	With spin-density V_B (MeV)	With spin-density R_B (fm)	ΔV_B (MeV)	ΔR_B (fm)
$^{12}C+^{12}C$	36	6.43	7.50	6.45	7.50	0.02	0.00
$^{12}C+^{18}O$	48	8.02	8.08	8.05	7.98	0.03	−0.10
$^{12}C+^{24}Mg$	72	11.47	8.33	11.53	8.33	0.06	0.00
$^{12}C+^{30}Si$	84	13.02	8.61	13.08	8.51	0.06	−0.10
$^{16}O+^{24}Mg$	96	15.05	8.53	15.07	8.43	0.02	−0.10
$^{24}Mg+^{26}Mg$	144	20.76	9.17	20.88	9.07	0.12	−0.10
$^{24}Mg+^{34}S$	192	27.25	9.29	27.37	9.29	0.12	0.00
$^{26}Mg+^{32}S$	192	27.13	9.30	27.29	9.20	0.16	−0.10
$^{28}Si+^{28}Si$	196	27.89	9.20	28.12	9.10	0.23	−0.10
$^{20}Ne+^{40}Ca$	200	28.59	9.21	28.64	9.21	0.05	0.00
$^{30}Si+^{58}Ni$	392	51.74	9.99	52.10	9.89	0.36	−0.10
$^{30}Si+^{64}Ni$	392	50.95	10.19	51.22	10.09	0.27	−0.10
$^{32}S+^{58}Ni$	448	59.29	9.94	59.70	9.84	0.41	−0.10
$^{40}Ar+^{58}Ni$	504	64.97	10.22	65.28	10.22	0.31	0.00
$^{40}Ar+^{64}Ni$	504	64.01	10.42	64.22	10.42	0.21	0.00
$^{58}Ni+^{58}Ni$	784	98.15	10.46	99.03	10.26	0.88	−0.20
$^{58}Ni+^{64}Ni$	784	96.67	10.66	97.30	10.56	0.63	−0.10
$^{64}Ni+^{64}Ni$	784	95.25	10.87	95.69	10.77	0.44	−0.10
$^{48}Ca+^{90}Zr$	800	96.88	10.96	97.33	10.86	0.45	−0.10

momentum, we get

$$\mathbf{J}_{n_v}(\mathbf{r})=\frac{n_v\mathbf{r}}{4\pi r^4}[j(j+1)-l(l+1)-\tfrac{3}{4}]R_l^2(r)\ . \qquad (16)$$

Here, l and j refer to the shell containing the n_v nucleons. Since a core consists of α-closed shells and for a closed shell $n_v=2j+1$, we get from (16)

$$\mathbf{J}_C(\mathbf{r})=\frac{\mathbf{r}}{4\pi r^4}\sum_\alpha (2j_\alpha+1)[j_\alpha(j_\alpha+1) -l_\alpha(l_\alpha+1)-\tfrac{3}{4}]R_\alpha^2(r)\ . \qquad (17)$$

This equation gives $\mathbf{J}=0$ for a nucleus with completely filled major shells, i.e., both $j=l\pm\frac{1}{2}$ shells filled. For the nucleon density ρ in Eq. (12) for $V_J(R)$ we have also used the Fermi density (10) since, as stated before, the shell-model density match very well the Fermi density, at least in the physically interesting tail region. The calculated $V_J(R)$ are also identical [15] for the two density distributions.

Finally, on adding the Coulomb potential V_C $(=Z_1Z_2e^2/R)$ to nuclear potential V_N, we get $V(R)$ which gives the height V_B and position R_B of the interaction barrier for each target and projectile combination.

III. CALCULATIONS

In this section, we discuss our calculations of fusion barrier heights and positions, their dependences on masses and charges of colliding nuclei, and use in calculations of excitation functions. Our calculations are compared with the available data and other model calculations. Also, the contribution of spin-density-dependent potential on fusion cross sections is analyzed.

A. Fusion barriers

Table I gives our results of calculation for the barrier heights and positions, using Skyrme interaction SIII with $\lambda=0$, compared with available empirical estimates and

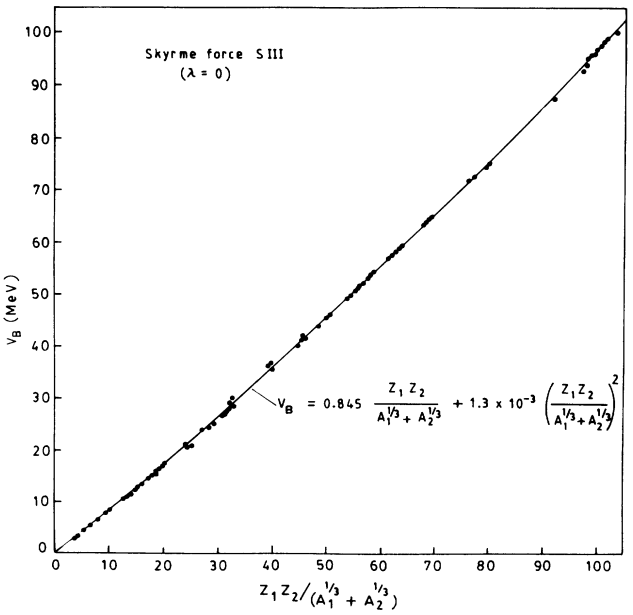

FIG. 5. The variation of our calculated barrier height V_B with $Z_1Z_2/(A_1^{1/3}+A_2^{1/3})$ for a large number of reactions. The solid line is a best fit to the data in terms of a second order polynomial.

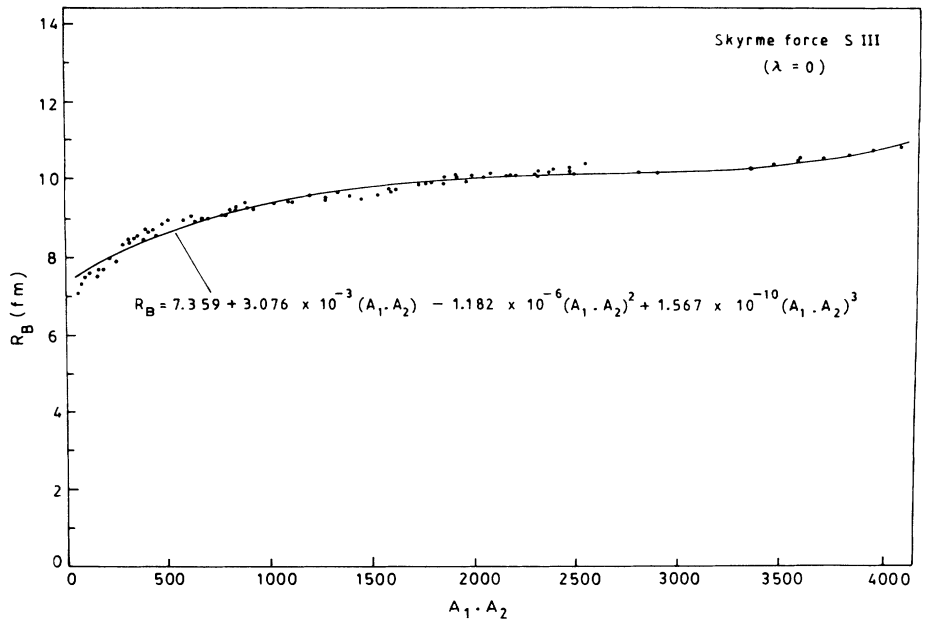

FIG. 6. The variation of our calculated barrier position R_B with $A_1 A_2$ for a large number of reactions. The solid line is a least-squares fit with a polynomial of degree three.

theoretical calculations based on models other than EDF. Table II gives a similar comparison with other available calculations using the EDF and Skyrme force SIII. The contribution of spin-density-dependent potential is, however, not present in these earlier calculations based on EDF. Our results clearly show that we are able to reproduce the empirical barrier heights V_B better and within ± 1 MeV. This is further demonstrated in Fig. 2 where $V_B^{\text{calculated}}$ is plotted versus $V_B^{\text{empirical}}$. The straight-line description of the data in this figure clearly shows the success of our model calculation. We have carried out this comparison further by comparing in Table III and Fig. 3 the barrier height predictions of the various model calculations. The data are taken from Vaz *et al.* [8]. Once again the deviations, $V_B^{\text{calculated}} - V_B^{\text{empirical}}$, lie closest to zero in our case. Figure 4, however, depicts that the situation does not remain the same when we compare our calculations of barrier positions R_B with the empirical

TABLE V. Comparisons for the interaction barriers, calculated on the actual (marked exact) and the simple analytical formula, using Skyrme force SIII ($\lambda=0$).

	Exact		Analytical			Exact		Analytical	
System	V_B	R_B	V_B	R_B	System	V_B	R_B	V_B	R_B
$^{12}C+^{12}C$	6.45	7.50	6.72	7.78	$^{26}Mg+^{34}S$	27.00	9.40	27.41	9.26
$^{12}C+^{16}O$	8.41	7.70	8.56	7.91	$^{28}Si+^{28}Si$	28.12	9.10	28.63	9.12
$^{12}C+^{18}O$	8.05	7.98	8.39	7.97	$^{28}Si+^{58}Ni$	52.67	9.73	52.14	9.91
$^{12}C+^{26}Mg$	11.34	8.44	11.83	8.21	$^{28}Si+^{62}Ni$	52.06	9.90	51.44	9.96
$^{12}C+^{28}Si$	13.20	8.45	13.65	8.27	$^{30}Si+^{30}Si$	27.54	9.31	27.94	9.28
$^{12}C+^{30}Si$	13.08	8.51	13.47	8.32	$^{30}Si+^{58}Ni$	52.10	9.89	51.57	9.96
$^{12}C+^{40}Ar$	16.38	8.84	16.45	8.58	$^{30}Si+^{62}Ni$	51.51	10.05	50.89	10.00
$^{16}O+^{16}O$	10.97	7.90	10.94	8.07	$^{32}S+^{40}Ca$	44.30	9.50	44.06	9.69
$^{16}O+^{20}Ne$	12.81	8.37	13.22	8.23	$^{32}S+^{58}Ni$	59.70	9.84	58.99	10.00
$^{16}O+^{24}Mg$	15.07	8.43	15.42	8.38	$^{32}S+^{64}Ni$	58.68	10.05	57.83	10.05
$^{16}O+^{26}Mg$	14.83	8.64	15.20	8.45	$^{34}S+^{58}Ni$	59.04	9.94	58.40	10.03
$^{16}O+^{28}Si$	17.25	8.55	17.56	8.51	$^{34}S+^{64}Ni$	58.06	10.24	57.27	10.07
$^{16}O+^{40}Ar$	21.42	8.94	21.25	8.89	$^{36}S+^{58}Ni$	58.45	10.13	57.85	10.06
$^{16}O+^{40}Ca$	23.98	8.94	23.71	8.89	$^{40}Ar+^{58}Ni$	65.28	10.22	64.63	10.09
$^{18}O+^{24}Mg$	14.55	8.71	15.13	8.48	$^{40}Ar+^{60}Ni$	64.95	10.25	64.20	10.10
$^{20}Ne+^{40}Ca$	28.64	9.21	28.93	9.14	$^{40}Ca+^{40}Ca$	54.26	9.68	53.86	9.90
$^{24}Mg+^{24}Mg$	21.19	8.96	21.90	8.77	$^{40}Ca+^{48}Ca$	52.60	10.06	52.10	10.02
$^{24}Mg+^{28}Si$	24.39	8.98	25.02	8.94	$^{40}Ca+^{58}Ni$	73.16	10.02	72.57	10.09
$^{24}Mg+^{32}S$	27.68	9.09	28.08	9.10	$^{58}Ni+^{58}Ni$	99.03	10.26	98.90	10.30
$^{24}Mg+^{34}S$	27.37	9.29	27.77	9.17	$^{58}Ni+^{64}Ni$	97.30	10.56	97.07	10.51
$^{26}Mg+^{32}S$	27.29	9.20	27.71	9.19	$^{64}Ni+^{64}Ni$	95.69	10.77	95.30	10.90

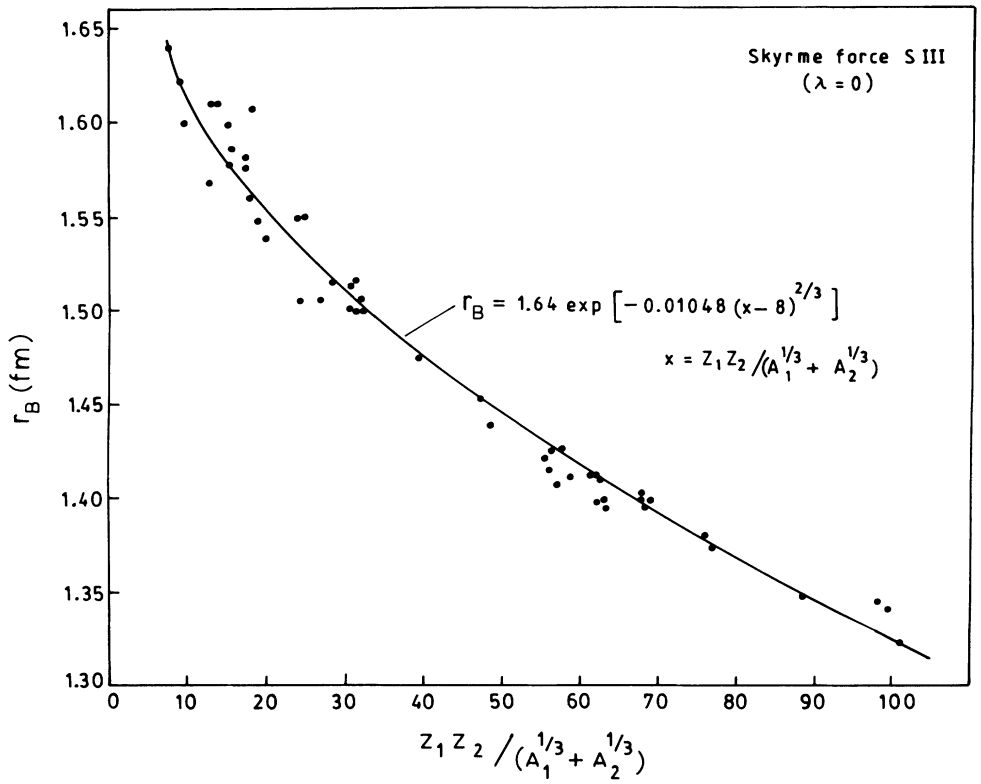

FIG. 7. Same as Fig. 5 but for r_B [$=R_B/(A_1^{1/3}+A_2^{1/3})$] instead of V_B. The best fit is in terms of an exponential function.

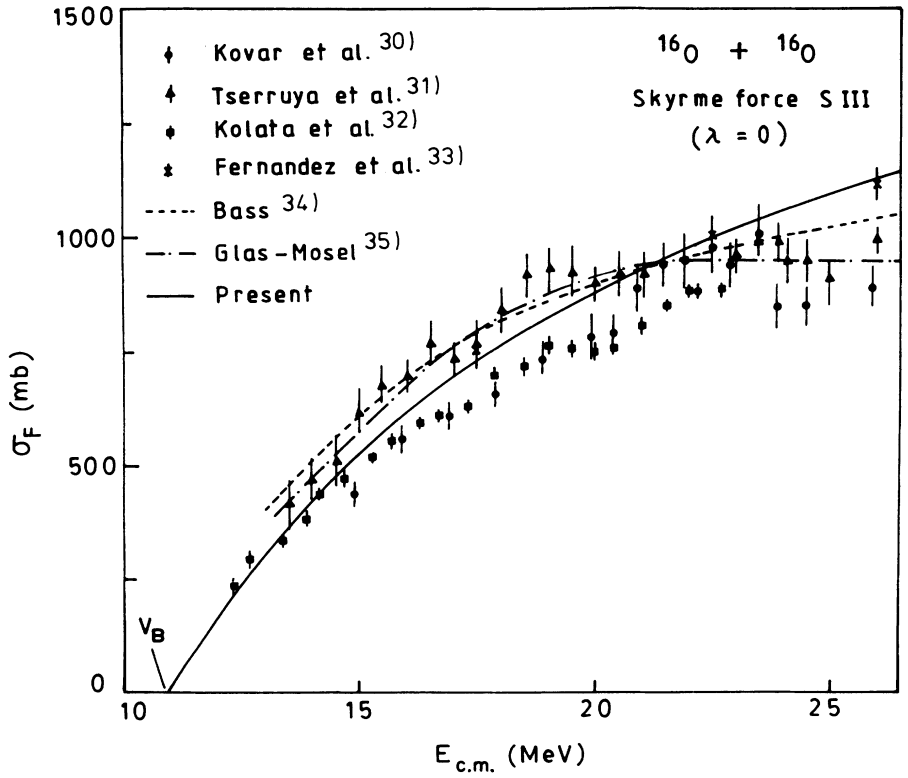

FIG. 8. Comparisons of our calculated excitation functions with the available experimental data [30–33] and other model calculations [34,35], for $^{16}O+^{16}O$ reaction.

data (Table I). The straight-line description is now rather approximate and does not go through the origin. In this context, it is relevant to note that the empirical data for fusion barriers are also always obtained in a model-dependent way [8].

In Table I, we have also listed our calculated Coulomb and nuclear potentials, V_C and V_N, respectively, at $R=R_B$. We observe that V_N increases as Z_1Z_2 increases. This is an expected result [11], since for larger Z_1Z_2 values, more and more nuclear interactions are needed to balance the Coulomb repulsion.

Finally, in Table IV we have analyzed the effects of the spin-density-dependent term V_J in the potential V_N on the barrier heights and positions. We notice that the effect of spin-density term on barrier height V_B is to increase it by as much as ~ 1 MeV ($\sim 1\%$) and shift the barrier position R_B (inside) by 0.1–0.2 fm. The barrier height seems to increase (almost) consistently with increasing Z_1Z_2 value. The interesting point is that such small changes in V_B and R_B due to V_J result in a decrease of fusion cross sections by as much as ~ 50 mb. This is discussed further in Sec. III C.

B. Simple parametrization of fusion barriers

Figures 5 and 6 show the variations of barrier heights V_B and positions R_B with relevant quantities in terms of only the masses and charges of colliding nuclei. The height V_B is plotted as a function of $Z_1Z_2/(A_1^{1/3}+A_2^{1/3})$ since the major contribution to barrier comes from Coulomb potential. The choice of R_B as a function of A_1A_2 stems from our earlier experience [7] with a similar parametrization of the repulsive barrier position of spin-density-dependent potential $V_J(R)$. Both the figures show very little scatter of the data and are nicely represented by the second and third order polynomials, respectively, as

$$V_B=(0.845\pm 0.020)\frac{Z_1Z_2}{A_1^{1/3}+A_2^{1/3}} +(1.3\mp 0.25)\times 10^{-3}\left[\frac{Z_1Z_2}{A_1^{1/3}+A_2^{1/3}}\right]^2, \quad (18a)$$

$$R_B=7.359+3.076\times 10^{-3}(A_1A_2) -1.182\times 10^{-6}(A_1A_2)^2+1.567\times 10^{-10}(A_1A_2)^3 . \quad (18b)$$

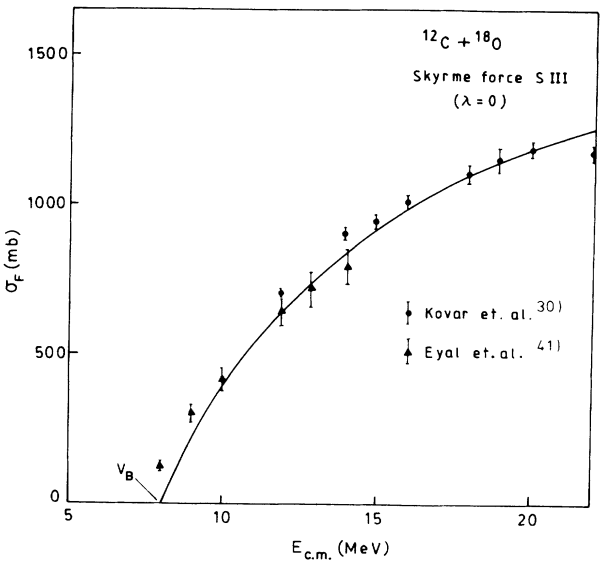

FIG. 10. Same as Fig. 8 but for $^{12}C+^{18}O$ reaction. The experimental data are from Refs. [30] and [41]. No other earlier calculation is available.

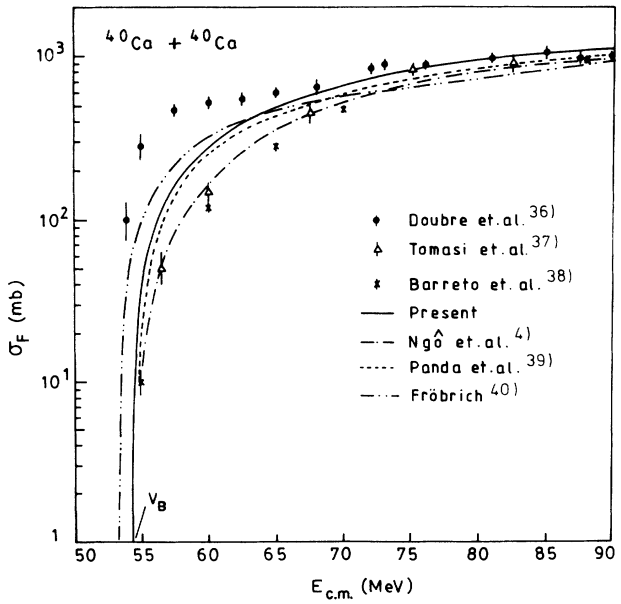

FIG. 9. Same as Fig. 8 but for $^{40}Ca+^{40}Ca$ reaction. The experimental data are from Refs. [36–38] and other model calculations are from Refs. [4,39,40].

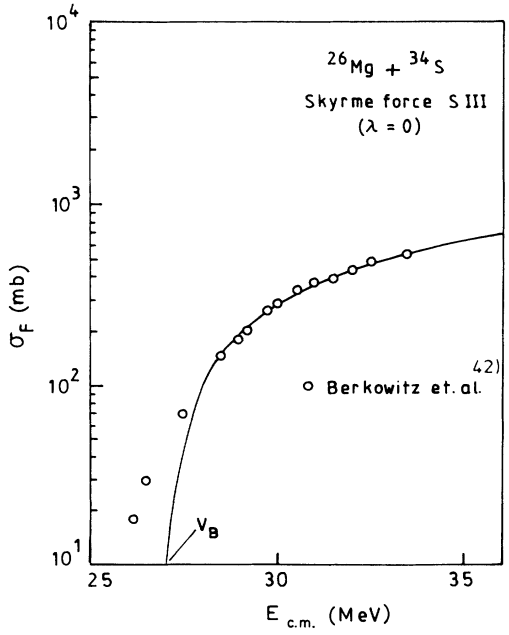

FIG. 11. Same as Fig. 10 but for $^{26}Mg+^{34}S$ reaction. The experimental data are from Ref. [42].

Equations (18a) and (18b) represent, respectively, a best fit and a least-squares fit to the data in Figs. 5 and 6. We have also attempted a least-squares fit to the data in Fig. 5 but that led to an unphysical result of negative barrier ($V_B = -0.9$ MeV, instead of zero) for zero Coulomb barrier. It is relevant to note that Eqs. (18) are obtained for light colliding nuclei with charges up to $Z=28$ and masses up to $A=64$ for each reaction partner.

We have also tested the accuracy of Eqs. (18). This is illustrated in Table V. We notice that barrier heights are given within about 0.5 MeV and the barrier positions within ~ 0.25 fm. Ngô *et al.* [11] and later Brink and Stancu [12] have also suggested a similar but graphical method to calculate V_B and R_B. These authors plotted a parameter r_B $[=R_B/(A_1^{1/3}+A_2^{1/3})]$ as a function of $Z_1Z_2/(A_1^{1/3}+A_2^{1/3})$ and V_N at $R=R_B$ as a function of r_B. However, the parameter r_B as a function of $Z_1Z_2/(A_1^{1/3}+A_2^{1/3})$ shows a larger scatter of the calculated data around the mean curve, as illustrated in Fig. 7. Thus, Eqs. (18) give almost for the first time an analytical simple method to calculate the fusion barriers from the knowledge of only the masses and charges of reaction partners.

C. Fusion cross sections

As already mentioned in the Introduction, a first calculation of the fusion cross sections for spin-unsaturated nuclei is published as a short Comment in Ref. [16]. There we considered the reactions $^{16}O+^{48}Ca$, $^{40}Ca+^{48}Ca$, and $^{40}Ca+^{60}Ni$. In these reactions, one of the reaction partners is always a spin-saturated nucleus. Figures 8–11 present our calculations for another four reactions $^{16}O+^{16}O$, $^{40}Ca+^{40}Ca$, $^{12}C+^{18}O$, and $^{26}Mg+^{34}S$. The first two of these reactions involve only the spin-saturated nuclei, whereas the other two have both their reaction partners as spin-unsaturated nuclei. The first two cases of spin-saturated nuclei are of interest because of their controversial nature of experimental data. Our calcula-

TABLE VI. Calculated complete fusion cross sections for some systems of highly spin-unsaturated nuclei, at energies $E_{c.m.} > V_B$. The barrier heights are given in Table IV.

System	$E_{c.m.}$ (MeV)	σ_{fus} (mb) (without V_J)	σ_{fus} (mb) (with V_J)	System	$E_{c.m.}$ (MeV)	σ_{fus} (mb) (without V_J)	σ_{fus} (mb) (with V_J)
$^{28}Si+^{28}Si$	28.50	56.92	34.69	$^{58}Ni+^{58}Ni$	99.50	46.64	15.62
	29.00	101.79	78.95		100.00	63.60	32.08
	30.00	187.04	163.05		101.00	97.00	65.51
	31.00	266.80	241.72		102.00	129.76	96.31
	32.00	341.57	315.48		103.00	161.87	127.48
	33.00	411.80	384.76		104.00	193.37	158.06
	34.00	477.91	449.97		105.00	224.27	188.06
	35.00	540.24	511.46		106.00	254.59	217.48
	36.00	599.10	569.52		107.00	284.33	246.36
	37.00	654.78	624.45		108.00	313.53	274.71
	38.00	707.54	676.49		109.00	342.19	302.53
	39.00	757.58	725.86		110.00	370.34	329.84
	40.00	805.13	772.76		111.00	397.97	356.67
	41.00	850.36	817.37		112.00	425.11	383.02
	42.00	893.43	859.86		113.00	451.77	408.90
	43.00	934.50	900.38		114.00	477.96	434.33
	44.00	973.70	939.05		115.00	503.70	459.31
					116.00	528.99	483.87
$^{40}Ar+^{58}Ni$	65.50	26.55	11.02		117.00	553.85	508.00
	66.00	51.22	35.80				
	67.00	99.43	84.25				
	68.00	146.23	131.27				
	69.00	191.67	176.93				
	70.00	235.82	221.29				
	71.00	278.72	264.39				
	72.00	320.00	306.30				
	73.00	360.99	347.06				
	74.00	400.46	386.72				
	75.00	438.88	425.32				
	76.00	476.29	462.90				
	77.00	512.72	499.51				
	78.00	548.22	535.18				
	79.00	582.83	569.95				
	80.00	616.56	603.85				
	81.00	649.47	636.91				

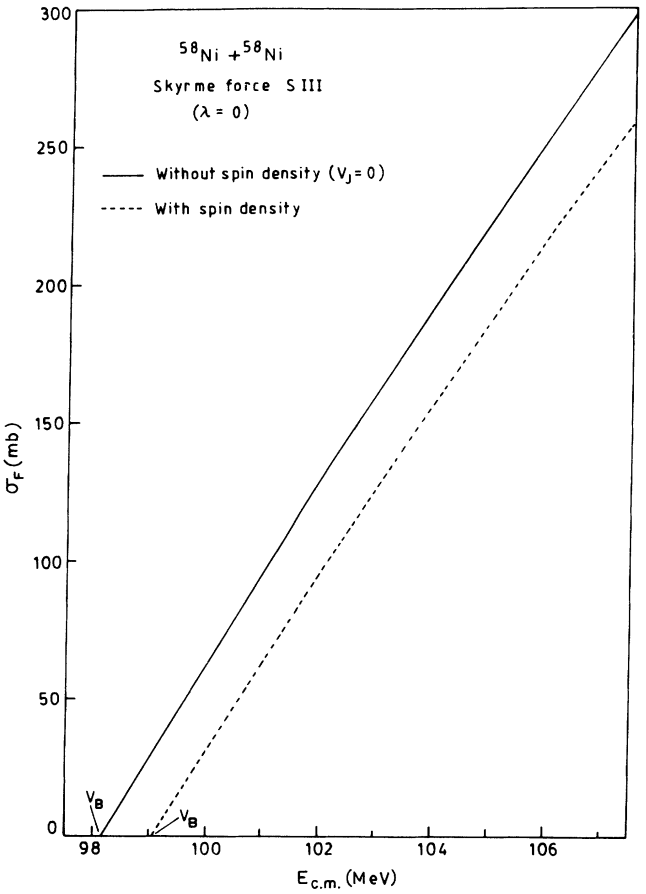

FIG. 12. Calculated excitation functions for ^{58}Ni+^{58}Ni reaction, using Skyrme force SIII (λ=0) with and without spin-density effects.

tions for $E_{c.m.} \geq V_B$, using the sharp cutoff model expression (3), give the general trends of the experimental data rather nicely in all the four cases. For ^{16}O+^{16}O and ^{40}Ca+^{40}Ca reactions, in contrast to earlier calculations, our calculations do not fit one or the other experimental data, but support their average behavior.

Finally, in order to see the contribution of spin-density term on fusion cross sections, we have calculated $\sigma_f(E_{c.m.} \geq V_B)$, with and without spin-density contribution, for the reactions ^{28}Si+^{28}Si, ^{40}Ar+^{58}Ni, and ^{58}Ni+^{58}Ni. The results of this calculation are presented in Table VI. These reactions use rather highly spin-unsaturated nuclei. We notice that fusion cross sections decrease with the addition of spin-density contribution and these effects increase more and more as we go towards the highly spin-unsaturated system like ^{58}Ni+^{58}Ni. This is further illustrated in Fig. 12 for the case of ^{58}Ni+^{58}Ni, where the cross sections are shown to decrease by as much as $\sim$50 mb due to the addition of spin-density effects in the potential. This is apparently a large effect for comparisons with experimental data.

IV. SUMMARY

We have used the energy-density model, based on density-dependent Skyrme interaction, for calculating the fusion barriers within the sudden approximation. The spin-density effects are also included. Our calculations are made for light nuclei (each nucleus with $Z \leq 40, A \leq 90$) and both the closed and unclosed shell nuclei are considered. We find that our calculated barrier heights lie within about $\pm$1 MeV of the empirical estimates. The role of spin density is found to increase the barrier heights by as much as $\sim$1 MeV and shift the barriers inside by 0.1–0.2 fm. Such seemingly small changes in barrier heights and positions are found to decrease the fusion cross sections by as much as $\sim$50 mb. The fusion cross sections, calculated within the sharp cutoff model for $E_{c.m.} \geq V_B$, are shown to be in nice agreement with experiments. Finally, simple analytical formulas are obtained which allow us to estimate the fusion barrier heights within an accuracy of $\sim$0.5 MeV and positions within $\sim$0.25 fm, simply from the masses and charges of colliding nuclei.

This work was supported in part by the Department of Science and Technology, and the Council of Scientific and Industrial Research, Govt. of India.

[1] H. Holm, W. Scheid, and W. Greiner, Phys. Lett. **29B**, 473 (1969); H. Holm and W. Greiner, Phys. Rev. Lett. **24**, 404 (1970).
[2] A. S. Jensen and C. Y. Wong, Phys. Lett. **32B**, 567 (1970); C. Y. Wong, *ibid.* **42B**, 186 (1972).
[3] R. K. Gupta, A Săndulescu, and W. Greiner, Phys Lett. **67B**, 257 (1977).
[4] C. Ngô, B. Tamain, M. Beiner, R. J. Lombard, D. Mas, and H. M. Deubler, Nucl. Phys. **A252**, 237 (1975).
[5] H. Ngô and C. Ngô, Nucl. Phys. **A348**, 140 (1980).
[6] D. M. Brink and Fl. Stancu, Nucl. Phys. **A299**, 321 (1978).
[7] R. K. Puri and R. K. Gupta, Int. J. Mod. Phys. E (to be published).
[8] L. C. Vaz, J. M. Alexander, and G. R. Satchler, Phys. Rep. **69**, 373 (1981).
[9] Tu. Ts. Oganessian, A. G. Demin, A. S. Iljinov, S. P. Tretyakova, A. A. Pleve, Yu. E. Penionzhkevich, M. P. Ivanov, and Yu. P. Tretyakova, Nucl. Phys. **A239**, 157 (1975); **A239**, 353 (1975).
[10] J. Galin, D. Guerreau, M. Lefort, and X. Tarrago, Phys. Rev. C **9**, 1018 (1974).
[11] C. Ngô, B. Tamain, J. Galin, M. Beiner, and R. J. Lombard, Nucl. Phys. **A240**, 353 (1975).
[12] Fl. Stancu and D. M. Brink, Nucl. Phys. **A270**, 236 (1976).
[13] K. A. Brueckner, J. R. Buchler, and M. M. Kelly, Phys. Rev. **173**, 944 (1968).
[14] D. Vautherin and D. M. Brink, Phys. Rev. C **5**, 626 (1972).
[15] R. K. Puri, P Chattopadhyay, and R. K. Gupta, Phys. Rev. C **43**, 315 (1991).
[16] R. K. Puri and R. K. Gupta, J. Phys. G **17**, 1933 (1991).
[17] R. K. Puri and R. K. Gupta, Proc. Nucl. Phys. Symp. (India) **33B**, 213 (1990).

[18] See, e.g., the recent review: R. K. Gupta, Invited Talk at International Conference on Nuclear and Atomic Clusters, Turku, Finland, 1991 (Springer-Verlag, Berlin, in press).
[19] R. Aroumougame, N. Malhotra, S. S. Malik, and R. K. Gupta, Phys. Rev. C **35**, 994 (1987).
[20] T. H. R. Skyrme, Nucl. Phys. **9**, 615 (1959).
[21] M. Beiner, H. Flocard, N. van Giai, and P. Quentin, Nucl. Phys. **A238**, 29 (1975).
[22] S. Köhler, Nucl. Phys. **A162**, 385 (1971); **A170**, 88 (1971).
[23] H. Krivine, J. Treiner, and H. Bohigas, Nucl. Phys. **A336**, 155 (1980).
[24] M. Brack, C. Guet, and H. Håkansson, Phys. Rep. **123**, 275 (1985).
[25] M. Rayet, M. Arnould, F. Tondeur, and G. Pauless, Astron. Astrophys. **116**, 183 (1982).
[26] C. M. Ko, H. C. Pauli, M. Brack, and G. E. Brown, Nucl. Phys. **A236**, 269 (1974).
[27] C. F. von Weizsäcker, Z. Phys. **96**, 431 (1935).
[28] J. Blocki, J. Randrup, W. J. Swiatecki, and C. F. Tsang, Ann. Phys. (N.Y.) **105**, 427 (1977).
[29] K. C. Panda and T. Patra, J. Phys. G **16**, 593 (1990).
[30] D. G. Kovar, D. F. Geesaman, T. H. Braid, Y. Eisen, W. Henning, T. R. Ophel, M. Paul, K. E. Rehm, S. J Sanders, P. Sperr, J. P. Schiffer, S. L. Tabor, S. Vigdor, B. Zeidman, and F. W. Prosser, Jr., Phys. Rev. C **20**, 1305 (1979).
[31] I. Tserruya, Y. Eisen, D. Pelte, A. Gavron, H. Oeschler, D. Berndt, and H. L. Harney, Phys. Rev. C **18**, 1688 (1978).
[32] J. J. Kolata, R. M. Freeman, F. Haas, B. Heusch, and A. Gallmann, Phys. Rev. C **19**, 2237 (1979).
[33] F. Fernandez, C. Gaarde, J. S. Larsen, S. Pontoppidan, and F . Videbaek, Nucl. Phys. **A306**, 259 (1978).
[34] R. Bass, Nucl. Phys. **A231**, 45 (1974).
[35] D. Glas and U. Mosel, Phys. Rev. C **10**, 2620 (1974); Phys. Lett. **49B**, 301 (1974); Nucl. Phys. **A237**, 429 (1975).
[36] H. Doubre, A. Gamp, J. C. Jacmart, N. Poffé, J. C. Roynette, and J. Wilczyński, Phys. Lett. **73B**, 135 (1978).
[37] E. Tomasi, D. Ardouin, J. Barreto, V. Bernard, B. Cauvin, C. Magnago, C. Mazur, C. Ngô, E. Piasecki, and M. Ribrag, Nucl. Phys. **A373**, 341 (1982).
[38] J. Barreto, G. Auger, M. Langevin, and F. Plagnol, Phys. Rev. C **27**, 1335 (1983).
[39] K. C. Panda, J. Phys. G **11**, 1323 (1985).
[40] P. Fröbrich, Phys. Rep. **116**, 337 (1984).
[41] Y. Eyal, M. Beckerman, R. Chechik, Z. Fraenkel, and H. Stöcker, Phys. Rev. C **13**, 1527 (1976).
[42] G. M. Berkowitz, P. Braun-Munzinger, J. S. Karp, R. H. Freifelder, J. R. Renner, and H. W. Wilschut, Phys. Rev. C **28**, 667 (1983).
[43] R. Rascher, W. F. J Müller, and K. P. Lieb, Phys. Rev. C **20**, 1028 (1979).
[44] C. M. Jachcinski, D. G. Kovar, R. R. Betts, C. N. Davids, D. F. Geesaman, C. Olmer, M. Paul, S. J. Sanders, and J. L. Yntema, Phys. Rev. C **24**, 2070 (1981).
[45] S. Gary and C. Volant, Phys. Rev. C **25**, 1877 (1982).
[46] Q. Haider and F. B. Malik, Phys. Rev. C **26**, 162 (1982).
[47] P. Basu, P. Bhattacharya, and M. L. Chatterjee, Pramăna J. Phys. **33**, 481 (1989).
[48] D. Shapira, D. DiGregorio, J. G. del Campo, R. A. Dayras, J. L. C. Ford, Jr., A. H. Snell, P H. Stelson, R. G. Stockstad, and F. Pougheon, Phys. Rev. C **28**, 1148 (1983).
[49] N. V. Sen, R. D. Blanc, J. C. Gondrand, and F. Merchez, Phys. Rev. C **20**, 969 (1979).
[50] E. F. Aguilera, J. J. Kolata, P. A. DeYoung, and J. J. Vega, Phys. Rev. C **33**, 1961 (1986).
[51] W. Scobel, H. H. Gutbrod, M. Blann, and A. Mignerey, Phys. Rev. C **14**, 1808 (1976).
[52] H. Esbensen, S. H. Fricke, and S. Landowne, Phys. Rev. C **40**, 2046 (1989).
[53] H. A. Aljuwair, R. J. Ledoux, M. Beckerman, S. B. Gazes, J. Wiggins, E. R. Cosman, R. R. Betts, S. Saini, and O. Hansen, Phys. Rev. C **30**, 1223 (1984).
[54] T. Udagawa, B. T. Kim, and T. Tamura, Phys. Rev. C **32**, 124 (1985).
[55] A. M. Stefanini, G. Fortuna, R. Pengo, W. Meczynski, G. Montagnoli, L. Corradi, A. Tivelli, S. Beghini, C. Signorini, S. Lunardi, M. Morando, and F. Soramel, Nucl. Phys. **A456**, 509 (1986).
[56] U. Jahnke, H. H. Rossner, D. Hilscher, and E. Holub, Phys. Rev. Lett. **48**, 17 (1982).
[57] M. Beckerman, M. Salomaa, A. Sperduto, J. D. Molitoris, and A. DiRienzo, Phys. Rev. C **25**, 837 (1982).
[58] B. Behera, K. C. Panda, and R. K. Satpathy, Phys. Rev. C **20**, 683 (1979).